



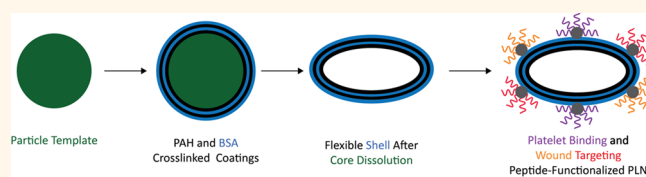
ARRCI
J

Platelet-like Nanoparticles: Mimicking Shape, Flexibility, and Surface Biology of Platelets To Target Vascular Injuries

Aaron C. Anselmo,[†] Christa Lynn Modery-Pawlowski,[‡] Stefano Menegatti,[†] Sunny Kumar,[†] Douglas R. Vogus,[†] Lewis L. Tian,[‡] Ming Chen,[†] Todd M. Squires,[†] Anirban Sen Gupta,[‡] and Samir Mitragotri^{*†}

[†]Department of Chemical Engineering, Center for Bioengineering University of California, Santa Barbara, California 93106, United States and [‡]Department of Biomedical Engineering Case Western Reserve University, Cleveland, Ohio 44106, United States

ABSTRACT Targeted delivery of therapeutic and imaging agents in the vascular compartment represents a significant hurdle in using nanomedicine for treating hemorrhage, thrombosis, and atherosclerosis. While several types of nanoparticles have been developed to meet this goal, their utility is limited by poor circulation, limited



margination, and minimal targeting. Platelets have an innate ability to marginate to the vascular wall and specifically interact with vascular injury sites. These platelet functions are mediated by their shape, flexibility, and complex surface interactions. Inspired by this, we report the design and evaluation of nanoparticles that exhibit platelet-like functions including vascular injury site-directed margination, site-specific adhesion, and amplification of injury site-specific aggregation. Our nanoparticles mimic four key attributes of platelets, (i) discoidal morphology, (ii) mechanical flexibility, (iii) biophysically and biochemically mediated aggregation, and (iv) heteromultivalent presentation of ligands that mediate adhesion to both von Willebrand Factor and collagen, as well as specific clustering to activated platelets. Platelet-like nanoparticles (PLNs) exhibit enhanced surface-binding compared to spherical and rigid discoidal counterparts and site-selective adhesive and platelet-aggregatory properties under physiological flow conditions *in vitro*. *In vivo* studies in a mouse model demonstrated that PLNs accumulate at the wound site and induce ~65% reduction in bleeding time, effectively mimicking and improving the hemostatic functions of natural platelets. We show that both the biochemical and biophysical design parameters of PLNs are essential in mimicking platelets and their hemostatic functions. PLNs offer a nanoscale technology that integrates platelet-mimetic biophysical and biochemical properties for potential applications in injectable synthetic hemostats and vascularly targeted payload delivery.

KEYWORDS: platelets · synthetic cells · layer-by-layer · nanotechnology · hemostat · vascular targeting

Nanoparticle-based therapies offer several advantages over free drugs including enhanced targeting and reduced off-target side effects.^{1–3} However, applications of nanoparticles are limited by rapid clearance due to immune-recognition and reduced targeting due to nonspecific binding.^{4–6} Several approaches based on synthesis of novel materials have been developed to address these challenges, and some of them have yielded exciting results at preclinical and early clinical stages.^{7,8} Bioinspired design approaches have recently emerged as a novel paradigm to address the limitations of classical nanoparticles.⁹ Specifically, natural circulating cells including erythrocytes, leukocytes, and platelets routinely perform functions of circulation and targeting that are often

desired in synthetic nanoparticles. Inspired by the superior functionality of innate circulatory cells, bioinspired strategies aim to impart some of the essential functional biological attributes into synthetic systems. For example, RBC-mimetic synthetic particles have been developed that mimic the shape and mechanical properties of RBCs to exhibit prolonged circulation.¹⁰ As another example, leukocyte-mimetic particles, coated with membranes of natural leukocytes on synthetic scaffolds, have been prepared and shown to accumulate in tumors.¹¹

Here, we report the synthesis of platelet-like nanoparticles (PLNs) and their ability to target an injured vascular site to render hemostasis. Targeted delivery of nanoparticles to vascular injury sites has been actively

* Address correspondence to samir@engineering.ucsb.edu.

Received for review July 8, 2014 and accepted October 15, 2014.

Published online October 15, 2014
10.1021/nn503732m

© 2014 American Chemical Society

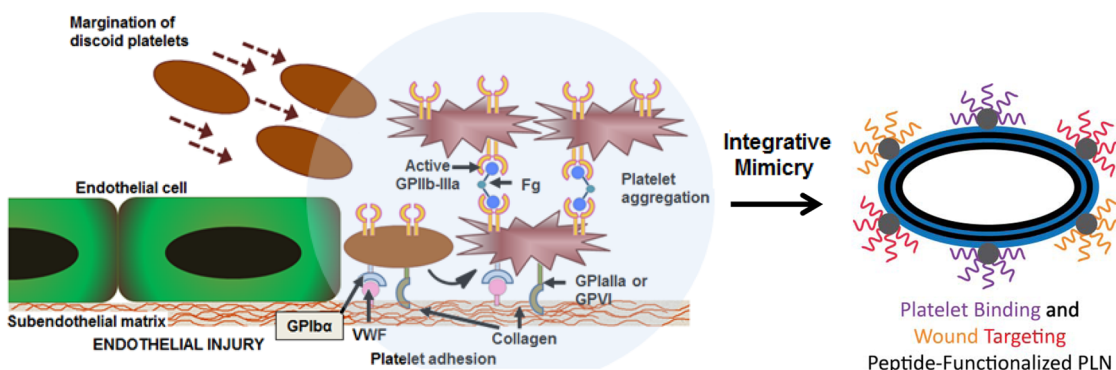


Figure 1. Platelet interactions in hemostasis and corresponding platelet-inspired design of PLN technology. Schematic showing normal hemostatic interactions that inspire PLN design.

researched owing to the nanoparticle's potential to treat various vascular disorders including cancer, inflammation, thrombosis, and hemorrhage.¹² Nanoparticles comprising various materials^{13,14} and targeting moieties^{3,15} have been used to specifically target vascular inflammation,¹⁶ vascular plaque,¹⁷ and clots.¹⁸ However, these nanoparticles possess attributes that are starkly different from circulating cells, especially platelets, which have evolved to expertly perform many of these functions.

Attempts have been made in the past to mimic certain aspects of platelet-related vascular targeting.^{19–27} Earlier approaches focused on liposomes or other polymeric particles functionalized with fibrinogen or fibrinogen-derived peptide ligands.²⁸ However, these approaches significantly deviate from the principles by which natural platelets function in two main ways. First, they do not mimic the complex biochemical interactions that occur when natural platelets interact with and bind to the endothelium.²⁸ Platelets circulate in a quiescent state and bind reversibly to the injured endothelium first *via* interaction with endothelium-secreted von Willebrand Factor (VWF) under high shear and then undergo stable adhesion *via* interaction with collagen. Platelets then become activated to trigger subsequent aggregation of other locally activated platelets *via* fibrinogen-mediated interactions with activated platelet integrin GPIIb-IIIa. Together, these synergistic adhesive and aggregatory interactions effectively form a hemostatic plug which halts bleeding. Second, liposomes and other polymeric particles do not mimic the biophysical discoid shape or the flexibility of natural platelets that are both essential in facilitating hemodynamic transport and margination of platelets toward endothelium to effectively render injury-site selective binding.²⁹ Our PLNs incorporate these often ignored biophysical design criteria of platelet-mimetic discoid morphology and flexibility and integrate these design parameters with the platelet-mimetic biochemical heteromultivalent interactive functions by dendritic presentation of multiple peptides that bind simultaneously to both activated

natural platelets and injured endothelial sites to promote injury-specific binding and hemostasis (Figure 1).

RESULTS

Synthesis and Characterization of PLNs. PLNs were synthesized using the layer-by-layer (LbL) approach^{30,31} (Figure 2a) to yield flexible capsules³² that are morphologically similar to natural platelets. Briefly, spherical polystyrene (PS) nanoparticles (Figure 2bi) were coated with complementary layers of poly(allylamine hydrochloride) (PAH) and bovine serum albumin (BSA) until 4 bilayers, $(\text{PAH}/\text{BSA})_4$, were formed on the template PS particle (Figure 2bii). PAH and BSA were chosen as the polycation and polyanion, respectively, due to their reliability in capsule synthesis *via* LbL³³ as well as their use as materials for numerous biomedical applications.^{34–37} PLNs (Figure 2biii) were characterized at each step for sufficient PAH/BSA coating (Figure 2c) *via* fluorimetric assays. Poly(allylamine hydrochloride)—AlexaFluor 594 (PAH-AF594) and bovine serum albumin—AlexaFluor 488 (BSA-AF488) were complementarily coated, and the fluorescent intensity for each dye was determined at each coating layer. The linear relationship of independently labeled polyelectrolytes with the number of layers implies the presence, and successive uniform coating, of both PAH and BSA.³⁸ The coating was further confirmed qualitatively *via* confocal imaging of the final PLN product (Figure 2c, inset). PS core removal was performed *via* incubation with tetrahydrofuran (THF) and isopropyl alcohol (IPA), at increasing THF/IPA ratios, and confirmed *via* FTIR (Figure 2d and Figure 1, Supporting Information) by monitoring absorbance at wavenumbers 700 and 760 cm^{-1} , which represent the mono-substituted benzene rings in polystyrene.³⁹ PLNs composed of $(\text{PAH}/\text{BSA})_4$ collapse into flexible discoidal particles following core removal (Figure 2biii). This change in shape results from the flexibility of the polymer/protein shell material collapsing onto itself since there is no longer a rigid PS core to maintain the original spherical structure (Figure 2bi). Previous studies involving the synthesis of LbL capsules utilizing

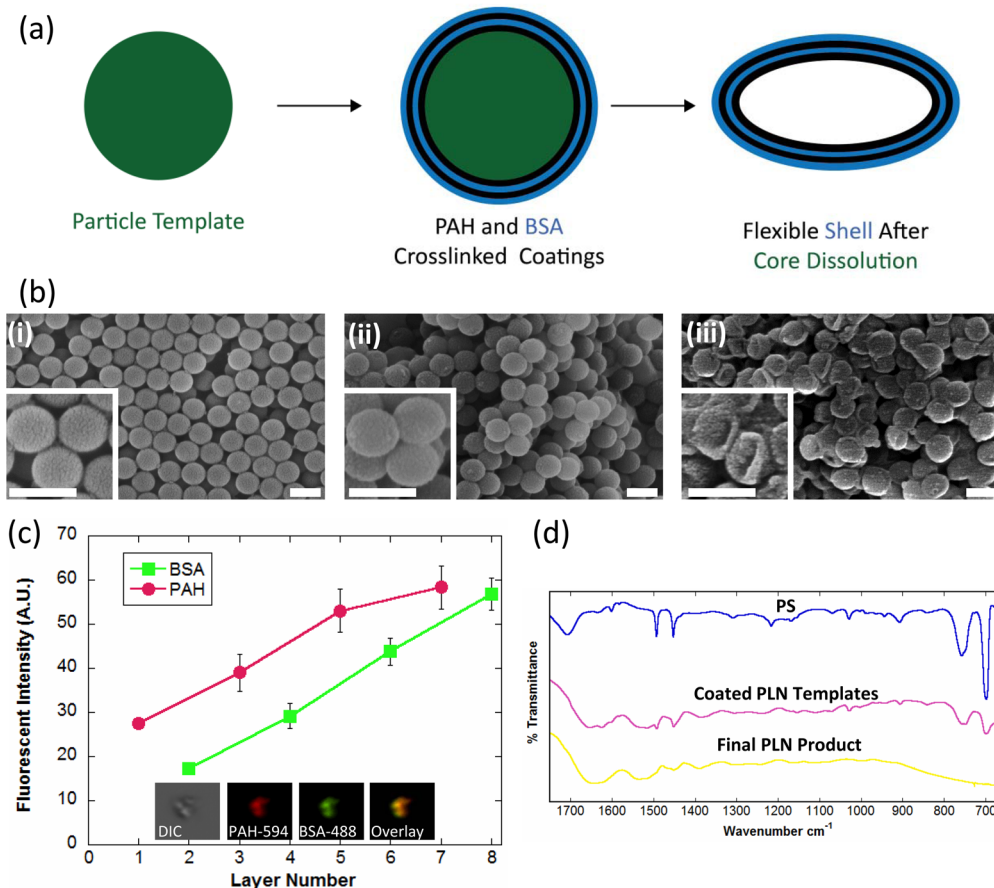


Figure 2. Synthesis and characterization of PLNs. (a) Schematic showing the LbL synthesis of PLNs. Note that the schematic shows only two bilayers of PAH/BSA, whereas four bilayers of PAH/BSA were used in this study. (b) Scanning electron micrographs (SEM) of (i) sacrificial 200 nm spherical polystyrene templates, (ii) $(\text{PAH}/\text{BSA})_4$ -coated polystyrene templates, and (iii) final PLNs. Scale bars = 200 nm. (c) Complementary coatings of poly(allylamine hydrochloride)-AlexaFluor 594 (odd layers) and bovine serum albumin-AlexaFluor 488 (even layers) with confocal imaging of final PLNs. (d) FTIR spectra of PS templates, $(\text{PAH}/\text{BSA})_4$ coated templates, and PLNs.

similar procedures, and materials have confirmed the softness of such particles.³²

Adhesion and Aggregation of PLNs Under Flow. The role of PLN's size and shape in determining their adhesion under flow conditions was assessed using microfluidic devices (Figure 3a inset; see Figure 2 (Supporting Information) for dimensions and uniformity of protein coating). Devices were coated with antiovalbumin (anti-OVA) antibody, and particles were coated with ovalbumin (OVA). OVA/anti-OVA interaction was used as a model antigen–antibody system. OVA-coated spherical particles of three sizes (200 nm, 1 μm , and 2 μm) were used to investigate the effect of particle size on shear-dependent adhesion. Larger spherical particles adhered in smaller quantities and consequently covered less surface area than their smaller counterparts (Figure 3a), a finding consistent with literature reports⁴⁰ that is likely due to the stronger shear detachment forces experienced by larger particles under flow.⁴¹

The shape of particles also impacted their adhesion on targeted surfaces. Since smaller particles adhered in higher quantities than their larger counterparts,

200 nm OVA-coated spheres, OVA-coated rigid discs stretched from 200 nm spheres and 200 nm OVA-coated flexible PLNs were studied under the same conditions as described above. Discoidal particles (discs, PLNs) covered more surface area of coated channels (Figure 3b) than their spherical counterpart, likely due to increased surface area contact of discoidal particles. Furthermore, PLNs covered more surface area than discs, likely due to their flexibility,³² which increases opportunities for multiligand interactions.¹² While spheres and discs adhere mostly as individual particles, PLNs appear to adhere as both individual and aggregates of particles adhering under shear (Figure 3b).

In view of their superior binding properties, 200 nm PLNs were used for further studies. This specific size also helps avoid cardiopulmonary interference. Specifically, particles similarly sized or larger than lung capillaries are known to physically get trapped in lungs (the first capillary bed encountered following tail vein injection) which can impede the passage of blood, effectively impairing oxygen delivery.^{2,42}

Peptide Conjugation to PLNs. PLNs were heteromultivalently surface-decorated with the collagen-binding

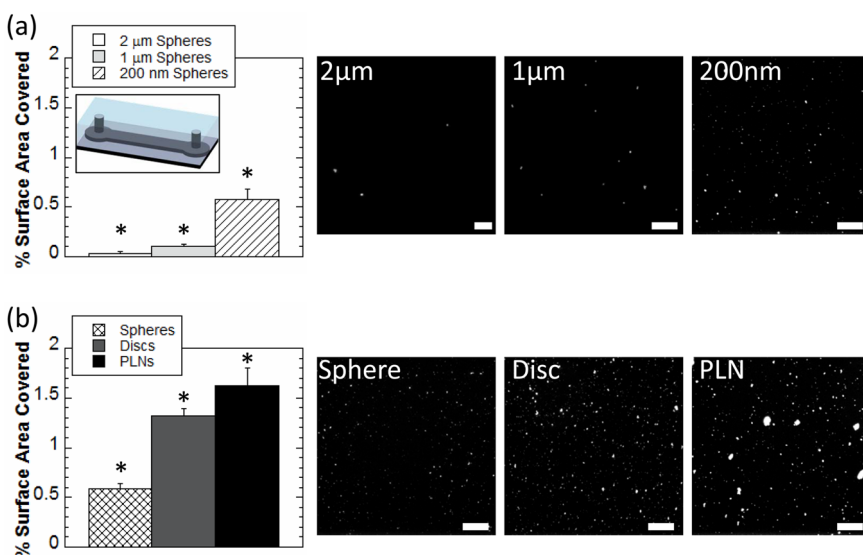


Figure 3. Particle binding. (a) Percentage of surface area coverage of OVA-coated spherical particles of 200 nm (white), 1 μm (light gray), and 2 μm (hatched) diameter to anti-OVA coated microfluidic channel (inset) under flow. (b) Percentage of surface area coverage of 200 nm OVA-coated spheres (cross-hatched), discs stretched from 200 nm spheres (gray) and 200 nm PLNs (black) to anti-OVA coated microfluidic channels (inset) under flow (see Figure 2a (Supporting Information) for device dimensions). Representative image scale bars = 20 μm . At least 10 images for each condition were used for analysis. *Denotes statistical difference ($P < 0.05$) from all other groups.

peptide (CBP; **[GPO]₇**) which binds to exposed collagen at the wound site *via* helicogenic interactions,⁴³ the von Willebrand Factor binding peptide (VBP; **TRYLRIHPQSQVHQI**) which binds to VWF⁴⁴ at the injury site, and the linear fibrinogen-mimetic peptide (FMP; **GRGDS**) which specifically binds to integrin GPIIb-IIIa on activated natural platelets^{45,46} to amplify platelet aggregation for hemostatic plug formation. These three peptide-mediated mechanisms act synergistically to promote injury-dependent site-specific stable adhesion, thereby allowing PLNs to localize at the injury site and then enhance platelet aggregation at that site *via* FMP. This integration of adhesion and aggregation functions are a significant refinement over past platelet substitute designs.²⁸ To ensure that peptides do not detach from PLNs *in vivo*, the three peptide ligands were covalently coupled to PLNs. Further, to avoid nonspecific interactions with the albumin-rich surface on PLNs and to increase the strength of selectivity of their respective binding, the peptides were not homogeneously coupled onto the surface of PLNs but instead were conjugated to branched dendrimers to form dendrimer-peptide structures on the surface of PLNs. Briefly, carboxyl-terminated (PAMAM) dendrimers were activated *via* carbonyldiimidazole (CDI), washed to remove excess CDI, reacted in individual flasks with the N-terminus of each of the three peptides, and finally washed to separate unreacted peptides from dendrimer-peptide conjugates (Figure 3a, Supporting Information). The outer layer of PLNs were enriched with primary amino groups by activation with CDI, followed by washing to remove excess CDI, addition of excess diaminoethane,

and finally washing to remove unreacted diaminoethane from amine-rich PLNs (Figure 3b, Supporting Information). Dendrimer-peptide conjugates were then activated *via* EDC chemistry, washed to remove excess EDC, and conjugated to PLNs to form stable amide bonds between the carboxyl rich dendrimer-peptide conjugates and the amine-rich PLN surface (Figure 3ci, Supporting Information; see Figure 3cii, Supporting Information, for final PLN schematic). Peptide conjugation to PLNs was quantified *via* fluorescent labeling of dendrimers (Figure 3d, Supporting Information) and confirmed qualitatively *via* confocal microscopy (Figure 3e, Supporting Information). PLN size ($235 \pm 4 \text{ nm}$) and surface charge ($-16 \pm 1 \text{ mV}$) were minimally altered following conjugation with dendrimer-peptides ($240 \pm 8 \text{ nm}$ and $-25 \pm 5 \text{ mV}$).

Aggregation and Adhesion of PLNs with Wound-Specific Ligands and Activated Platelets under Flow *in Vitro*. The platelet-mimetic adhesive and aggregatory capabilities of the PLNs were assessed *in vitro* in a parallel plate flow chamber (PPFC) setup (Figure 4, Supporting Information). For adhesion studies, glass slides were coated with adjacent regions of BSA (negative control surface) and 50:50 VWF/collagen (positive control surface). Green fluorescent unmodified PLNs and VBP + CBP PLNs, which should bind specifically to the VWF/collagen surface, were allowed to flow over these coated glass slides in the PPFC at both physiological and pathological wall shear stresses^{18,47} of $5\text{--}55 \text{ dyn/cm}^2$ for 45 min. Adhesion of targeted and nontargeted PLNs to both targeted and nontargeted surfaces was imaged and quantified (Figure 4a). Indeed, unmodified PLNs had minimal adhesion on the

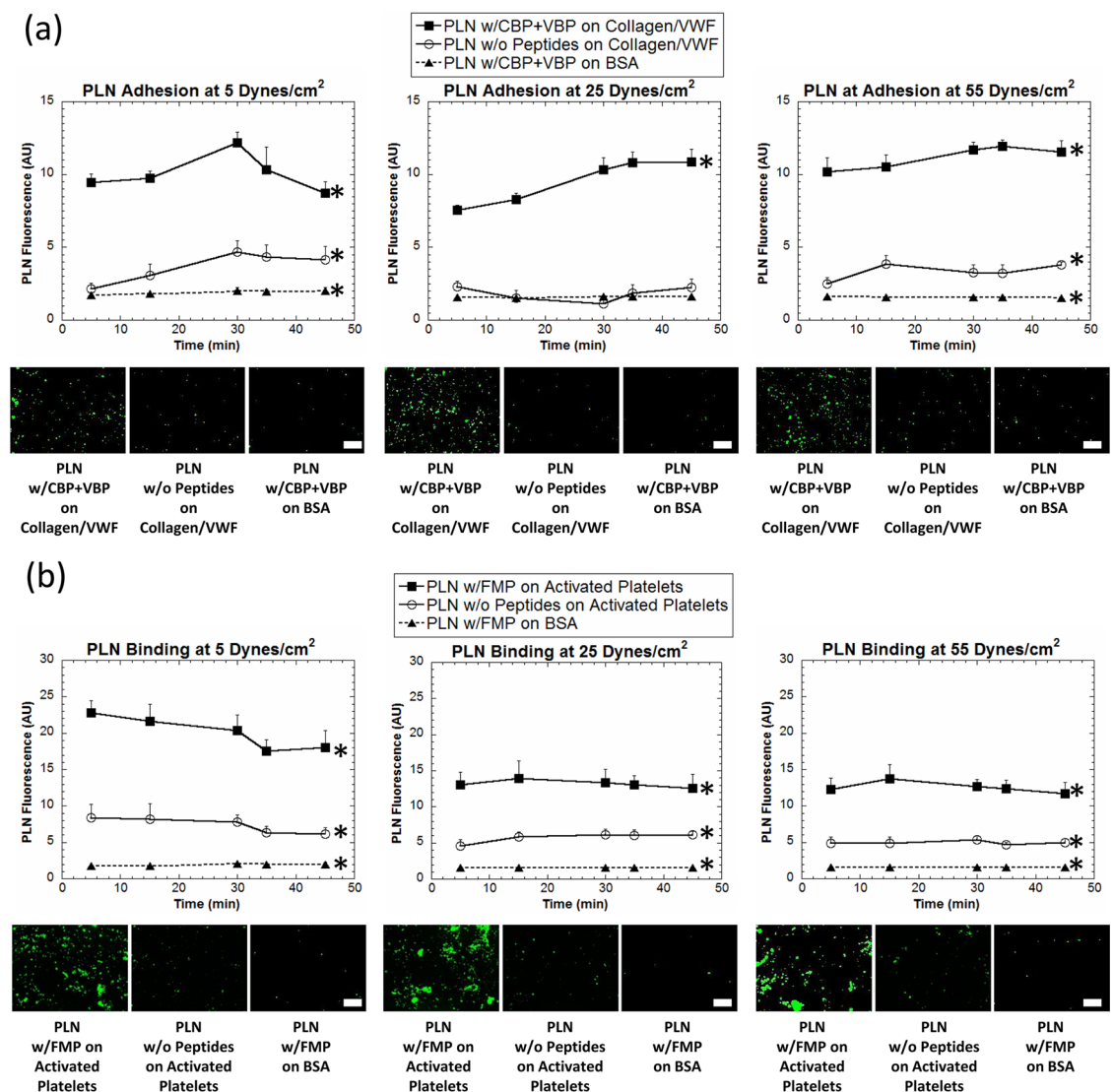


Figure 4. *In vitro* binding of PLNs at various shear stresses. (a) PLNs modified with CBP + VBP show specific adhesion to VWF–collagen-coated surfaces (filled squares), PLNs without peptide modification show minimal adhesion to VWF–collagen-coated surfaces (circles), and PLNs modified with CBP + VBP show minimal adhesion to nontargeted control BSA surfaces (filled triangles) in a parallel plate flow chamber (PPFC) at various shear values. Representative images are shown for the end of the experiment (45 min) for each condition. At least 10 images at for each condition at each time were used for analysis. Scale bars = 50 μ m. (b) PLNs modified with FMP aggregate with natural platelets (filled squares), PLNs without peptide modification show minimal aggregation with natural platelets (circles), and PLNs modified with FMP show minimal aggregation with nontargeted control BSA surfaces (filled triangles) in a PPFC at various shear values. Representative images are shown for the end of the experiment (45 min) for each condition. At least 10 images at for each condition at each time were used for analysis. Scale bars = 50 μ m. All images were taken at the same magnification. *Denotes statistical difference ($P < 0.05$) from all other groups at each time point.

VWF/collagen surface and peptide-modified PLNs had minimal adhesion on the control BSA surface. In comparison, the peptide-modified PLNs showed significantly enhanced adhesion on the VWF–collagen surface due to the specific synergistic interaction mechanisms of VBPs with VWF and CBPs with collagen. To study the interaction capabilities of PLNs with natural activated platelets, platelet-rich-plasma (PRP) was incubated in the presence of adenosine diphosphate (ADP), which facilitates the transition of unactivated platelets to activated platelets, with glass slides bearing BSA-coated and collagen-coated adjacent regions in order to

form a layer of activated platelets on the collagen-coated region but not on the BSA-coated region. Green fluorescent unmodified PLNs and FMP-modified PLNs, which should bind specifically to the activated platelets, were allowed to flow over these slide surfaces at wall shear stresses of 5–55 dyn/cm² for 45 min. Aggregation of PLNs with natural platelets was imaged and quantified (Figure 4b) at various wall shear stresses. FMP-PLNs showed significantly enhanced binding to the activated platelet-covered region, and minimal binding to non-targeted BSA surface, at all shear values. Furthermore, unmodified PLNs showed minimal adhesion to activated

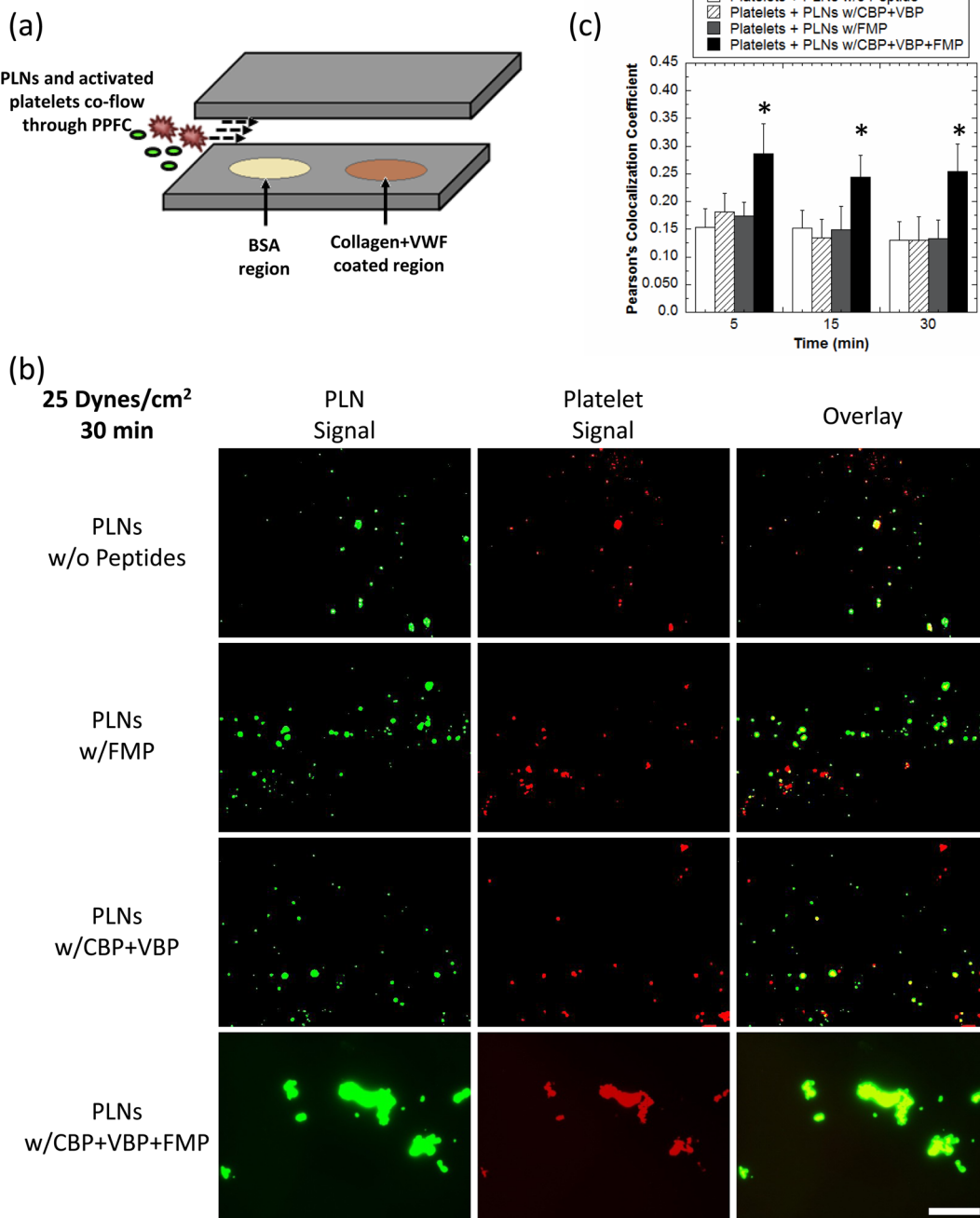


Figure 5. *In vitro* PLN wound adhesion and platelet aggregation in simulated wound environment. (a) Experimental setup for flowing PLNs and activated platelets together over VWF–collagen-coated surfaces. PLNs first encounter a BSA region so as to limit nonspecific binding at the collagen–VWF-coated surface. (b) PLNs are able to adhere to VWF–collagen-coated surfaces while aggregating with natural platelets in a PPFC better than PLNs with no peptides, FMP-only, or CBP + VBP-only. Representative images are shown for the end of the experiment (30 min) for each condition. Scale bar = 50 μ m. All images were taken at the same magnification. (c) Pearson's colocalization coefficient values for: (i) activated platelets + PLNs without peptides (white bars), (ii) activated platelets + PLNs with CBP + VBP modification (hatched bars), (iii) activated platelets + PLNs with FMP modification (gray bars), and (iv) activated platelets + PLNs with CBP + VBP + FMP modification (black bars). At least 10 images for each condition were used for analysis. *Denotes statistical difference ($P < 0.05$) from all other groups.

platelets. Collectively, these *in vitro* flow experiments highlight the ability of PLNs to present a variety of platelet-relevant targeting ligands that interact specifically with vascular target sites while minimally interacting with physically similar, nontargeted surfaces.

PLN Interaction and Clot Formation with Natural Platelets in an *In Vitro* Wound Model. The ability of PLNs to combine

both adhesion and aggregation on a single particle construct was tested in a simulated injury site environment. For these studies, human platelets (stained red) were preactivated with ADP and subjected to flow over BSA-coated (control surface that exhibits no specific binding to VBPs and CBPs) and VWF–collagen-coated (test surface with specific binding to VBPs and CBPs)

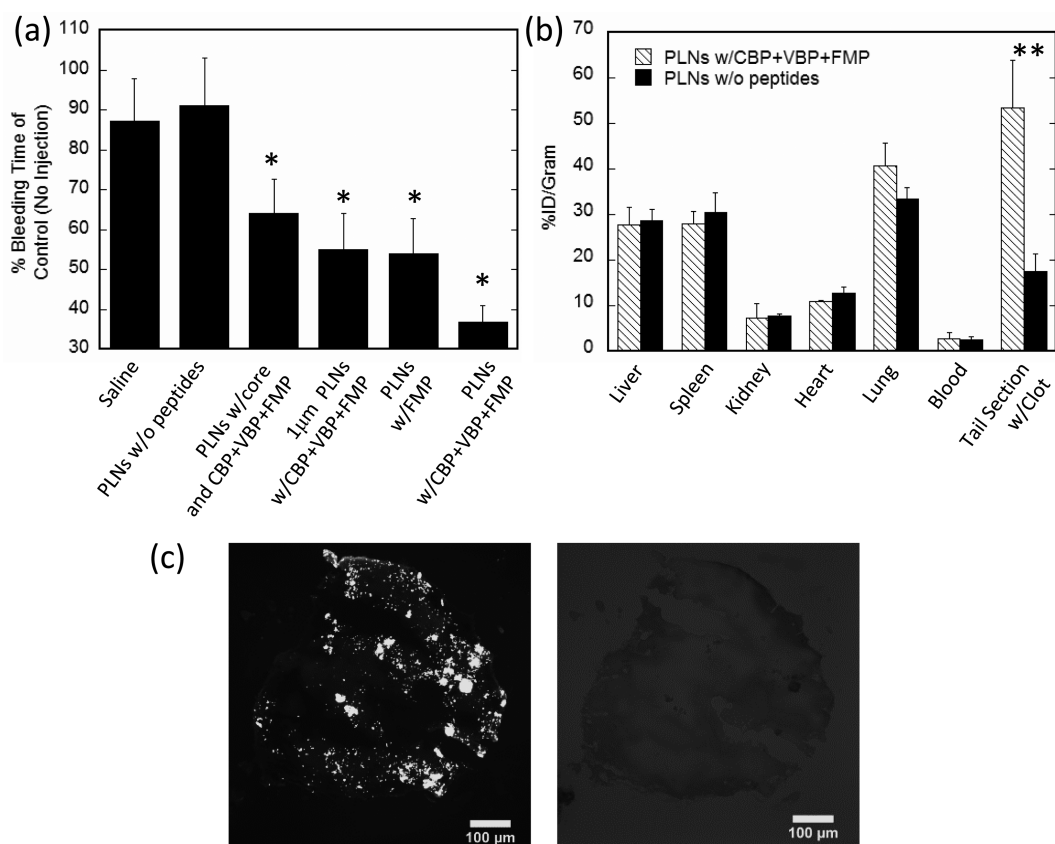


Figure 6. *In vivo* hemostatic effect, biodistribution, and imaging of PLNs in mouse tail transection model. (a) PLNs reduce bleeding times in a tail amputation model in mice. PLNs functionalized with CBP + VBP + FMP peptides reduce bleeding times by 65% compared to control (no injections). (b) Plain PLNs or PLNs functionalized with CBP + VBP + FMP organ distribution at 1 h or 55 min after tail amputation. (c) Brightfield and fluorescent images of tail section clot confirming fluorescently labeled CBP + VBP + FMP PLNs interacting with tail section clot. Scale bar = 100 μ m. *Denotes statistical difference ($P < 0.05$) from saline and PLNs without peptide controls. **Denotes statistical difference ($P < 0.05$) between PLN formulations in specific tissue.

regions (Figure 5a) at wall shear stress of 25 dyn/cm² along with the four formulations of green fluorescent PLNs, namely (i) unmodified PLNs, (ii) “adhesive only” CBP + VBP PLNs, (iii) “aggregatory only” FMP PLNs, or (iv) “functionally integrated” PLNs containing all three peptides (CBP + VBP + FMP). PLNs bearing all three peptides were most effective in adhering stably to the VWF–collagen surfaces while recruiting activated platelets, under a flow environment, to the adhesion site (Figure 5b). Indeed, “functionally integrated” PLNs showed significantly enhanced fluorescence colocalization with activated platelets, validating the synergistic effect of the three peptides in a single platelet-mimicking particle platform. Co-localization, which is the overlap of activated platelets (red) and PLNs (green), was quantified using multiple images for each group via Pearson’s coefficient (Figure 5c). This quantitative representation (Figure 5c) of images (Figure 5b) highlights the importance of combining both aggregation and adhesion platelet properties into a single PLN formulation in order to both adhere stably to wound-mimicking surfaces while recruiting activated platelets, or in other words, form a hemostatic plug.

While natural circulating platelets undergo complex shear-dependent aggregation at vascular injuries,^{48,49}

due in part to their discoidal shape and unique presentation of surface receptors that benefit from lateral mobility afforded by their flexibility, the majority of polymeric nanoparticles do not possess this ability. However, PLNs appear to undergo shear-dependent aggregation on targeted surfaces upon binding in all flow experiments performed (Figures 3, 4, and 5). To investigate shear-induced aggregation, PLNs were imaged before and after flow through a capillary. Before flow, PLNs are dispersed and show limited aggregation, while after experiencing shear under flow, PLNs form larger aggregates (Figure 5, Supporting Information). This suggests that the physical properties of PLNs allow for similar aggregation abilities that their natural counterparts routinely leverage to facilitate hemostasis.

In Vivo Hemostasis Effect and Biodistribution of PLNs. PLNs were next investigated *in vivo* for their ability to halt bleeding in a standard tail transection model in BALB/c mice. PLNs without peptides and saline injections alone showed no decrease in tail bleeding times. PLNs functionalized with only the FMP peptide (**GRGDS**) lowered bleeding time by ~45% (Figure 6a), which is comparable to results reported for past synthetic hemostat designs of particles bearing fibrinogen-based RGD or AGD peptides.²³ However, “functionally

integrated” PLNs (bearing all three peptides **GRGDS**, **TRYLRIHPQSQVHQI**, and **[GPO]₇**) lowered bleeding time by ~65%. Further, micron-sized “functionally integrated” PLNs were unable to instigate hemostasis to the same extent as their 200 nm counterparts, likely due to the lower circulation time of micron sized particles and also the less efficient binding and adhesion that larger particles exhibit under flow conditions. Nonflexible spherical 200 nm “functionally integrated” PLNs containing the rigid PS core were also unable to cause hemostasis as rapidly as the more flexible, disc-shaped PLNs, likely due to their limited aggregation at the wound site. Organ distribution for 200 nm PLNs with and without CBP + VBP + FMP peptide functionalization showed similar organ accumulation except in the case of the tail section containing the clot (Figure 6b). In this case, a 3-fold increase in PLNs functionalized with CBP + VBP + FMP peptides in the tail section containing the clot was seen over unmodified PLNs. Targeting of “functionally integrated” PLNs to tail clots was confirmed *via* fluorescent imaging (Figure 6c). Images of the clot show that PLNs bind in aggregates (Figure 6c) as predicted by *in vitro* flow experiments (Figures 3–5). Histology sections of liver, brain, and lungs were taken at 24 h following injections of either saline (control) or functionally integrated PLNs (Figure 6, Supporting Information). Histopathology indicated slightly increased occurrence of microthrombi in lungs in case of PLNs compared to controls, likely due to lung accumulation (Figure 6b). The liver and brain tissues showed no pathologies for either group.

DISCUSSION

The results shown here demonstrate the ability of bioinspired PLNs to significantly reduce the bleeding time in a mouse tail transection model. PLNs were synthesized *via* the LbL method for precise control over their size, shape, and material composition. Similar to their natural counterpart, PLNs were discoidal in shape and were functionalized with wound-specific and platelet-specific peptides (see Figure 3 (Supporting Information) for activation and reaction schematic, peptide quantification, and PLN imaging) so as to mimic the biochemical interactions of natural platelets with both injured endothelium and each other. Both biophysical and biochemical design parameters of PLNs were investigated for their role in adhesion under physiological flow conditions. First, the biophysical design parameters of PLNs, namely their discoidal shape and flexible exterior, showed individual and aggregated PLN binding to targeted surfaces under flow. PLNs were then independently assessed for their specific adhesion to both wound-specific ligands and to activated platelets under physiologically relevant flow conditions. PLNs functionalized with wound-specific ligands show high specific adhesion to collagen and VWF-coated slides

and limited interaction with negative control BSA surfaces. Similarly, PLNs functionalized with fibrinogen interacting peptides (**GRGDS**) showed high specific adhesion to activated platelet-coated surfaces and minimal adhesion to negative control BSA surfaces. In both cases, PLNs which had no peptide functionalization showed minimal adhesion to both collagen- and VWF-coated surfaces and activated platelet-coated surfaces. Furthermore, PLNs which had targeting peptides showed minimal adhesion to negative control BSA surfaces. Following this, an *in vitro* wound model confirmed that PLNs functionalized with both wound adhesive and activated platelet aggregatory peptides formed clots more efficiently than PLNs functionalized with adhesive only or aggregatory only peptides. In all binding studies, PLNs adhered to targeted surfaces as both individual particles and as larger aggregates. PLN aggregation stems from a combination of their physical and chemical features. PLN's ability to aggregate under shear was investigated *via* capillary flow experiments. Imaging of PLNs before, during, and after capillary flow, under high shear conditions, illustrates the ability of PLNs to undergo shear-dependent aggregation. We hypothesize that, much like real platelets, PLNs marginate to the wall under shear due to their physical parameters (e.g., shape and flexibility) and are likely to have higher local concentration at the wall under flow. This increase in local PLN concentration can potentially cause PLNs to interact with each other and clump together if shear conditions permit. Literature in colloidal physics field has shown that colloidal particles aggregate under shear owing largely to increased local concentration of particles.⁵⁰ The *in vitro* flow experiments accurately predicted the PLN clustering seen in the fluorescent histology tail sections.

In the case of normal hemostatic plug formation, circulating platelets become activated and bind to the damaged endothelium due to exposure of collagen and release of VWF from the wound site. In case of hemostatic plug formation following injection of PLNs, activated circulating platelets and PLNs both bind to injured endothelium, as well as to each other, effectively forming the hemostatic plug much faster than in the absence of PLNs. Brightfield and fluorescent images show the interaction between fluorescently labeled PLNs and the clot (Figure 6c), which was verified *via* biodistribution as functionalized PLNs accumulated 3-fold higher in the clot as compared to plain PLNs. Following an injection of PLNs, the hemostatic plug formed in ~35% of the time it took when no PLNs were injected. The importance of the biochemical design parameters were verified *in vivo* as platelet-aggregatory-only or wound-adhesive-only PLNs were unable to promote hemostasis as effectively as PLNs combining both functions. Furthermore, the importance of the biophysical design parameters were verified *in vivo* as rigid/spherical PLNs with both wound-adhesive

and platelet-aggregation abilities were unable to promote hemostasis as well as PLNs of discoidal shape. An increase in microthrombi was seen in histological lung sections in some cases following treatment with PLNs. This is likely due to increased overall activity of circulating platelets following tail transection compounded with the observed lung accumulation. To minimize these complications, a low PLN dose of 15 mg/kg was used as compared to much higher doses reported, often exceeding 50 mg/kg, that have been shown to induce cardiopulmonary issues in the form of elevated heart rates and gasping.²³ Such complications were not observed with the lower dose of PLNs used in this study.

Various cell mimetic^{10,32} and cell-inspired^{51–53} systems have been recently reported for a variety of biotechnology applications.⁹ The PLNs presented here combine many unique aspects of circulatory platelets, specifically their shape and surface chemistry interactions, to perform functions that are typically exclusive to natural platelets. The LbL technique used here is widely utilized for the synthesis of a variety of LbL particles with proven biomedical applications^{34,54,55}

and is ideal for fabricating synthetic cells as it allows for enhanced control over particle design. Furthermore, the PLNs described here will benefit from the recently reported scaled up synthesis of similarly fabricated LbL particles.³⁵ Future studies will be focused on translating the fast acting hemostatic ability of PLNs to larger, more serious wounds, determining the dose-dependent cardiopulmonary impact following PLN injection and assessment of the extent of complement activation following PLN injection. PLNs potentially offer a new intravenous tool for the treatment of severe bleeding and hemorrhage. Also, certain peptide-decorative subsets of PLNs, for example, the FMP-decorated designs, can be potentially used to target platelet-rich occlusive clot sites for site-specific delivery of fibrinolytic or antiplatelet agents which can reduce the systemic coagulopathy risks otherwise presented by such agents. Therefore, PLNs can become an effective technology not only as “synthetic hemo-stats”, but also a platform for tailoring targeted therapeutic actions in atherosclerosis, thrombosis, or restenosis in the vascular compartment.

METHODS

PLN Fabrication. Carboxylated PS spheres (200 nm) (Polysciences, Warrington, PA) were suspended in 0.5 M sodium chloride. Positively charged poly(allylamine hydrochloride) (2 mg/mL) (Sigma) was dissolved in 0.5 M sodium chloride and incubated with 12.5 mg of PS particles at room temperature under constant rotation for 30 min. Particles were then centrifuged at 15000g for 30 min and resuspended in 0.5 M sodium chloride. Particles were washed two more times at 15000g for 30 min in 0.5 M sodium chloride. Following PAH coating, negatively charged bovine serum albumin (Sigma) was coated on top of PAH layers under identical conditions. This procedure was repeated for four total PAH/BSA bilayers. Intermittent cross-linking with 2% glutaraldehyde (Polysciences) for 1 h under constant rotation was performed to ensure sufficient structural integrity of the outer shells. Following glutaraldehyde exposure, the particles were incubated in 30 mM sodium borohydride to stop the cross-linking reaction. The particles were then exposed to a tetrahydrofuran–isopropyl alcohol gradient (1:3, 1:2, 1:1, 2:1, and pure THF) for 30 min each at room temperature under constant rotation so as to dissolve the PS core. Particles were then washed 10 times with saline so as to remove any residual solvent and stored at 4 °C for no longer than 2 days.

In Vitro Studies: Microfluidic Experiments. Devices (see the Supporting Information for synthesis) were washed with saline and coated with 500 µg/mL of antiovalbumin monoclonal antibody at either 4 °C overnight or at 37 °C for 1 h. PLNs were prepared as described above, and discs were prepared using previously described film stretching methods.⁵⁶ All particles were terminally coated with 2 mg/mL of PAH for 30 min at room temperature, cross-linked with 2% glutaraldehyde as above, and then coated with 1 mg/mL of ovalbumin at 4 °C overnight. Particles were washed 3× in saline and resuspended at a concentration of 5×10^{11} particles/mL. Particles were subjected to flow, via syringe pump withdrawal, through the devices at a constant flow rate of 0.27 mL/h (shear rate of 800 s⁻¹ on bottom of channel) for 1 min and then washed with saline at 0.27 mL/h for 2 min to remove unbound particles. Devices were then imaged using an Andor iXON 885 fluorescent camera, and at least 10 images were analyzed for binding to channel surface by calculating total surface area covered using ImageJ. Surface

area coverage was quantified as opposed to quantity of particles since sufficient hemostatic plug formation requires complete wound plugging, which is dependent not on the quantity of particles but on the total area the particles can occupy.

Peptide Conjugation to PLNs. Succinamic acid terminated PAMAM dendrimers, generation 5.0 (Dendritech), were activated with carbonyldiimidazole (CDI) at 1 mg/mL in acetone. Removal of CDI from activated dendrimers was performed using Amicon centrifugal filters (3 kDa) for 3 washes. Each of the three peptides were then added and coupled to CDI activated dendrimers in separate flasks via their N-terminus. Removal of unreacted peptides from dendrimer-peptide conjugates was performed using Amicon centrifugal filters (3 kDa) for three washes. The outer layer of PLNs was activated with CDI at 1 mg/mL in acetone for 45 min. Free CDI was removed via centrifugation. Diaminoethane was then added to yield primary amino groups on PLN surface and purified via centrifugation. All PLNs were tested qualitatively for free amines via the Kaiser test. Finally, dendrimer-peptide conjugates were conjugated to PLNs via EDC chemistry in MES buffer at 4.5 pH for 12 h (see Figure 3a–c, Supporting Information, for stepwise activation and reaction scheme). For coupling of peptides to particles still containing polystyrene cores, particles were activated with EDC at 4 mg/mL in MES buffer for 10 min, washed to remove excess EDC, reacted with diaminoethane to form primary amino groups on the surface, and reacted with dendrimer-peptides via EDC chemistry.

In Vitro Studies of Hemostatically Relevant PLN Interactions. The interaction of peptide-modified PLNs with injury site-relevant proteins (VWF and collagen) and activated platelets in a flow environment was studied using a parallel plate flow chamber (PPFC) system connected with a programmable pump and recirculating loop with silicone tubing. The PPFC setup was placed under an inverted fluorescent microscope and the experimental surfaces were imaged over time to allow quantitative fluorescence intensity analysis of particle and cell interactions. The flow rate of particle and platelet suspensions in the PPFC was controlled by a programmable pump to allow a wall shear stress range of 5–55 dyn/cm² as per the equation $\tau_w = 6\mu Qb^{-1}h^{-2}$, where τ_w is the wall shear stress, Q is the flow rate, μ is the fluid viscosity (0.015 dyn/cm²), b is the PPFC chamber width (1.0 cm), and h is the distance between the PPFC plates

(0.00254 cm). The resultant shear stress range is within the physiological and pathological ranges of wall shear stresses in the vasculature. For image analysis, the fluorescence intensities of 10 images per time point per shear stress were analyzed using a MATLAB script, and statistical analyses were performed using ANOVA, with significance considered at $p < 0.05$. For the colocalization analyses between red fluorescent platelets and green fluorescent PLNs, an ImageJ (NIH) script called Just Another Co-localization Plugin (JACoP) was used that utilizes the Pearson's coefficient estimation of the association strength between two color channels in the image fluorescence histogram.

In Vivo Hemostasis. All experiments were performed as per approved protocols by the IACUC of the University of California, Santa Barbara. PLNs in saline (15 mg/kg) were injected via tail vein into healthy female BALB/c mice (18–20 g; $n = 3$ –6 per group). Five minutes after injection, 2 mm long sections of the tail, from the distill tip, were amputated. The amputated tail was immediately immersed in 14 mL of sterile saline at 37 °C. The times until bleeding from the amputated tail stopped were recorded with a stopwatch.

In Vivo Biodistribution. PLNs (15 mg/kg), either plain or conjugated with CBP + VBP + FMP peptides, in saline were injected via tail vein into healthy female BALB/c mice (18–20 g; $n = 3$ –6 per group). Five minutes following injection, 2 mm long sections of the tail, from the distill tip, were amputated. Fifty-five minutes following tail amputation, animals were sacrificed via CO₂ overdose and organs were collected. The organs were dissolved overnight in Solvable at a concentration of 100 mg of organ per 1 mL of Solvable. Dissolved organ solutions were measured for their fluorescence at a concentration of 2 mg of organ per 200 μL Solvable. Background fluorescent values of each organ, from control animals receiving no injection, were subtracted from each organ value for CBP + VBP + FMP PLN and plain PLN groups.

Conflict of Interest: The authors declare no competing financial interest.

Acknowledgment. A.C.A. was supported by the National Science Foundation Graduate Research Fellowship under Grant No. DGE-1144085. C.L.M. was supported by National Science Foundation Graduate Research Fellowship Program under Grant No. DGE-0951783. D.R.V. was supported by the National Science Foundation Graduate Research Fellowship under Grant No. DGE-1144085. A.S.G. is supported by NIH Grant No. 1R01HL121212-01. The MRL Central Facilities are supported by the MRSEC Program of the NSF under Award No. DMR 1121053, a member of the NSF-funded Materials Research Facilities Network (www.mrfn.org). We thank Michael Zakrewsky of UCSB for help with confocal microscopy.

Supporting Information Available: Additional material includes supporting figures, captions, methods, and references. This material is available free of charge via the Internet at <http://pubs.acs.org>.

REFERENCES AND NOTES

- Peer, D.; Karp, J. M.; Hong, S.; Farokhzad, O. C.; Margalit, R.; Langer, R. Nanocarriers as an Emerging Platform for Cancer Therapy. *Nat. Nanotechnol.* **2007**, *2*, 751–760.
- Moghim, S. M.; Hunter, A. C.; Murray, J. C. Long-Circulating and Target-Specific Nanoparticles: Theory to Practice. *Pharmacol. Rev.* **2001**, *53*, 283–318.
- Petros, R. A.; DeSimone, J. M. Strategies in the Design of Nanoparticles for Therapeutic Applications. *Nat. Rev. Drug Discovery* **2010**, *9*, 615–627.
- Riehemann, K.; Schneider, S. W.; Luger, T. A.; Godin, B.; Ferrari, M.; Fuchs, H. Nanomedicine—Challenge and Perspectives. *Angew. Chem., Int. Ed.* **2009**, *48*, 872–897.
- Sanhai, W. R.; Sakamoto, J. H.; Canady, R.; Ferrari, M. Seven Challenges for Nanomedicine. *Nat. Nanotechnol.* **2008**, *3*, 242–244.
- Owens, D. E., 3rd; Peppas, N. A. Opsonization, Biodistribution, and Pharmacokinetics of Polymeric Nanoparticles. *Int. J. Pharm.* **2006**, *307*, 93–102.
- Wang, A. Z.; Langer, R.; Farokhzad, O. C. Nanoparticle Delivery of Cancer Drugs. *Annu. Rev. Med.* **2012**, *63*, 185–198.
- Heidel, J. D.; Davis, M. E. Clinical Developments in Nanotechnology for Cancer Therapy. *Pharm. Res.* **2011**, *28*, 187–199.
- Yoo, J. W.; Irvine, D. J.; Discher, D. E.; Mitragotri, S. Bio-Inspired, Bioengineered and Biomimetic Drug Delivery Carriers. *Nat. Rev. Drug. Discovery* **2011**, *10*, 521–535.
- Merkel, T. J.; Jones, S. W.; Herlihy, K. P.; Kersey, F. R.; Shields, A. R.; Napier, M.; Luft, J. C.; Wu, H.; Zamboni, W. C.; Wang, A. Z.; et al. Using Mechanobiological Mimicry of Red Blood Cells to Extend Circulation Times of Hydrogel Microparticles. *Proc. Natl. Acad. Sci. U.S.A.* **2011**, *108*, 586–591.
- Parodi, A.; Quattracchi, N.; van de Ven, A. L.; Chiappini, C.; Evangelopoulos, M.; Martinez, J. O.; Brown, B. S.; Khaled, S. Z.; Yazdi, I. K.; Enzo, M. V.; et al. Synthetic Nanoparticles Functionalized with Biomimetic Leukocyte Membranes Possess Cell-Like Functions. *Nat. Nanotechnol.* **2013**, *8*, 61–68.
- Howard, M.; Zern, B. J.; Anselmo, A. C.; Shubaev, V. V.; Mitragotri, S.; Muzykantov, V. Vascular Targeting of Nanocarriers: Perplexing Aspects of the Seemingly Straightforward Paradigm. *ACS Nano* **2014**, *8*, 4100–4132.
- Doshi, N.; Mitragotri, S. Designer Biomaterials for Nanomedicine. *Adv. Funct. Mater.* **2009**, *19*, 3843–3854.
- Mitragotri, S.; Lahann, J. Materials for Drug Delivery: Innovative Solutions to Address Complex Biological Hurdles. *Adv. Mater.* **2012**, *24*, 3717–3723.
- Ruosahti, E. Peptides as Targeting Elements and Tissue Penetration Devices for Nanoparticles. *Adv. Mater.* **2012**, *24*, 3747–3756.
- Zern, B. J.; Chacko, A.-M.; Liu, J.; Greineder, C. F.; Blankemeyer, E. R.; Radhakrishnan, R.; Muzykantov, V. Reduction of Nanoparticle Avidity Enhances the Selectivity of Vascular Targeting and PET Detection of Pulmonary Inflammation. *ACS Nano* **2013**, *7*, 2461–2469.
- Nahrendorf, M.; Jaffer, F. A.; Kelly, K. A.; Sosnovik, D. E.; Aikawa, E.; Libby, P.; Weissleder, R. Noninvasive Vascular Cell Adhesion Molecule-1 Imaging Identifies Inflammatory Activation of Cells in Atherosclerosis. *Circulation* **2006**, *114*, 1504–1511.
- Korin, N.; Kanapathipillai, M.; Matthews, B. D.; Crescente, M.; Brill, A.; Mammo, T.; Ghosh, K.; Jurek, S.; Bencherif, S. A.; Bhatta, D. Shear-Activated Nanotherapeutics for Drug Targeting to Obstructed Blood Vessels. *Science* **2012**, *337*, 738–742.
- Coller, B. S.; Springer, K. T.; Beer, J. H.; Mohandas, N.; Scudder, L. E.; Norton, K. J.; West, S. M. Thromboerythrocytes. *In Vitro* Studies of a Potential Autologous, Semi-Artificial Alternative to Platelet Transfusions. *J. Clin. Invest.* **1992**, *89*, 546–555.
- Rybak, M. E.; Renzulli, L. A. A Liposome Based Platelet Substitute, the Plateletsome, with Hemostatic Efficacy. *Biomater., Artif. Cells, Immobilization Biotechnol.* **1993**, *21*, 101–118.
- Levi, M.; Friederich, P. W.; Middleton, S.; de Groot, P. G.; Wu, Y. P.; Harris, R.; Biemond, B. J.; Heijnen, H. F.; Levin, J.; ten Cate, J. W. Fibrinogen-Coated Albumin Microcapsules Reduce Bleeding in Severely Thrombocytopenic Rabbits. *Nat. Med.* **1999**, *5*, 107–111.
- Nishiya, T.; Kainoh, M.; Murata, M.; Handa, M.; Ikeda, Y. Reconstitution of Adhesive Properties of Human Platelets in Liposomes Carrying Both Recombinant Glycoproteins Ia/Ila and Ib Alpha Under Flow Conditions: Specific Synergy of Receptor-Ligand Interactions. *Blood* **2002**, *100*, 136–142.
- Bertram, J. P.; Williams, C. A.; Robinson, R.; Segal, S. S.; Flynn, N. T.; Lavik, E. B. Intravenous Hemostat: Nanotechnology to Halt Bleeding. *Sci. Transl. Med.* **2009**, *1*, 11ra22.
- Doshi, N.; Orje, J. N.; Molins, B.; Smith, J. W.; Mitragotri, S.; Ruggeri, Z. M. Platelet Mimetic Particles for Targeting Thrombi in Flowing Blood. *Adv. Mater.* **2012**, *24*, 3864–3869.
- Ravikumar, M.; Modery, C. L.; Wong, T. L.; Gupta, A. S. Peptide-Decorated Liposomes Promote Arrest and Aggregation of Activated Platelets Under Flow on Vascular Injury

- Relevant Protein Surfaces *in Vitro*. *Biomacromolecules* **2012**, *13*, 1495–1502.
26. Ravikumar, M.; Modery, C. L.; Wong, T. L.; Dzuricky, M.; Sen Gupta, A. Mimicking Adhesive Functionalities of Blood Platelets using Ligand-Decorated Liposomes. *Bioconjugate Chem.* **2012**, *23*, 1266–1275.
27. Modery-Pawlowski, C. L.; Tian, L. L.; Ravikumar, M.; Wong, T. L.; Sen Gupta, A. *In Vitro and in Vivo* Hemostatic Capabilities of a Functionally Integrated Platelet-Mimetic Liposomal Nanoconstruct. *Biomaterials* **2013**, *34*, 3031–3041.
28. Modery-Pawlowski, C. L.; Tian, L. L.; Pan, V.; McCrae, K. R.; Mitragotri, S.; Sen Gupta, A. Approaches to Synthetic Platelet Analogs. *Biomaterials* **2012**, *34*, 526–541.
29. Gentile, F.; Chiappini, C.; Fine, D.; Bhavane, R.; Peluccio, M.; Cheng, M.; Liu, X.; Ferrari, M.; Decuzzi, P. The Effect of Shape on the Margination Dynamics of Non-Neutrally Buoyant Particles in Two-Dimensional Shear Flows. *J. Biomech.* **2008**, *41*, 2312–2318.
30. Wang, Y.; Angelatos, A. S.; Caruso, F. Template Synthesis of Nanostructured Materials via Layer-by-Layer Assembly. *Chem. Mater.* **2007**, *20*, 848–858.
31. Zhou, Z.; Anselmo, A. C.; Mitragotri, S. Synthesis of Protein-Based, Rod-Shaped Particles from Spherical Templates using Layer-by-Layer Assembly. *Adv. Mater.* **2013**, *25*, 2723–2727.
32. Doshi, N.; Zahr, A. S.; Bhaskar, S.; Lahann, J.; Mitragotri, S. Red Blood Cell-Mimicking Synthetic Biomaterial Particles. *Proc. Natl. Acad. Sci. U.S.A.* **2009**, *106*, 21495–21499.
33. del Mercato, L. L.; Rivera-Gil, P.; Abbasi, A. Z.; Ochs, M.; Ganas, C.; Zins, I.; Sonnichsen, C.; Parak, W. J. LbL Multilayer Capsules: Recent Progress and Future Outlook for Their use in Life Sciences. *Nanoscale* **2010**, *2*, 458–467.
34. Johnston, A. P.; Cortez, C.; Angelatos, A. S.; Caruso, F. Layer-by-Layer Engineered Capsules and Their Applications. *Curr. Opin. Colloid Interface Sci.* **2006**, *11*, 203–209.
35. Yan, Y.; Björnalm, M.; Caruso, F. Assembly of Layer-by-Layer Particles and Their Interactions with Biological Systems. *Chem. Mater.* **2014**, *26*, 452–460.
36. Lee, E. S.; Kim, D.; Youn, Y. S.; Oh, K. T.; Bae, Y. H. A Virus-Mimetic Nanogel Vehicle. *Angew. Chem., Int. Ed.* **2008**, *47*, 2418–2421.
37. Lu, W.; Zhang, Y.; Tan, Y.-Z.; Hu, K.-L.; Jiang, X.-G.; Fu, S.-K. Cationic Albumin-Conjugated Pegylated Nanoparticles as Novel Drug Carrier for Brain Delivery. *J. Controlled Release* **2005**, *107*, 428–448.
38. Richardson, J. J.; Liang, K.; Kempe, K.; Ejima, H.; Cui, J.; Caruso, F. Immersive Polymer Assembly on Immobilized Particles for Automated Capsule Preparation. *Adv. Mater.* **2013**, *25*, 6874–6878.
39. Pastukhov, A. V.; Tsyurupa, M. P.; Davankov, V. A. Hyper-crosslinked Polystyrene: A Polymer in a Non-Classical Physical State. *J. Polym. Sci., Part B: Polym. Phys.* **1999**, *37*, 2324–2333.
40. Patil, V. R. S.; Campbell, C. J.; Yun, Y. H.; Slack, S. M.; Goetz, D. J. Particle Diameter Influences Adhesion Under Flow. *Biophys. J.* **2001**, *80*, 1733–1743.
41. Doshi, N.; Prabhakarpandian, B.; Rea-Ramsey, A.; Pant, K.; Sundaram, S.; Mitragotri, S. Flow and Adhesion of Drug Carriers in Blood Vessels Depend on Their Shape: A Study Using Model Synthetic Microvascular Networks. *J. Controlled Release* **2010**, *146*, 196–200.
42. Kutscher, H. L.; Chao, P.; Deshmukh, M.; Singh, Y.; Hu, P.; Joseph, L. B.; Reimer, D. C.; Stein, S.; Laskin, D. L.; Sinko, P. J. Threshold Size for Optimal Passive Pulmonary Targeting and Retention of Rigid Microparticles in Rats. *J. Controlled Release* **2010**, *143*, 31–37.
43. Mo, X.; An, Y.; Yun, C. S.; Yu, S. M. Nanoparticle-Assisted Visualization of Binding Interactions Between Collagen Mimetic Peptide and Collagen Fibers. *Angew. Chem., Int. Ed.* **2006**, *45*, 2267–2270.
44. Nogami, K.; Shima, M.; Giddings, J. C.; Takeyama, M.; Tanaka, I.; Yoshioka, A. Relationship Between the Binding Sites for von Willebrand Factor, Phospholipid, and Human Factor VIII C2 Inhibitor Alloantibodies Within the Factor VIII C2 Domain. *Int. J. Hematol.* **2007**, *85*, 317–322.
45. Pytela, R.; Pierschbacher, M. D.; Ginsberg, M. H.; Plow, E. F.; Ruoslahti, E. Platelet Membrane Glycoprotein IIb/IIIa: Member of a Family of Arg-Gly-Asp-Specific Adhesion Receptors. *Science* **1986**, *231*, 1559–1562.
46. Shoffstall, A. J.; Atkins, K. T.; Groynom, R. E.; Varley, M. E.; Everhart, L. M.; Lashof-Sullivan, M. M.; Martyn-Dow, B.; Butler, R. S.; Ustin, J. S.; Lavik, E. B. Intravenous Hemostatic Nanoparticles Increase Survival Following Blunt Trauma Injury. *Biomacromolecules* **2012**, *13*, 3850–3857.
47. Resnick, N.; Yahav, H.; Shay-Salit, A.; Shushy, M.; Schubert, S.; Zilberman, L. C. M.; Wofovitz, E. Fluid Shear Stress and the Vascular Endothelium: For Better and for Worse. *Prog. Biophys. Mol. Biol.* **2003**, *81*, 177–199.
48. Jackson, S. P. The Growing Complexity of Platelet Aggregation. *Blood* **2007**, *109*, 5087–5095.
49. Nesbitt, W. S.; Westein, E.; Tovar-Lopez, F. J.; Tolouei, E.; Mitchell, A.; Fu, J.; Carberry, J.; Fouras, A.; Jackson, S. P. A Shear Gradient-Dependent Platelet Aggregation Mechanism Drives Thrombus Formation. *Nat. Med.* **2009**, *15*, 665–673.
50. Genovese, D. B. Shear Rheology of Hard-Sphere, Dispersed, and Aggregated Suspensions, and Filler-Matrix Composites. *Adv. Colloid Interface Sci.* **2012**, *171*, 1–16.
51. Anselmo, A. C.; Gupta, V.; Zern, B. J.; Pan, D.; Zakrewsky, M.; Muzykantov, V.; Mitragotri, S. Delivering Nanoparticles to Lungs while Avoiding Liver and Spleen through Adsorption on Red Blood Cells. *ACS Nano* **2013**, *7*, 11129–11137.
52. Rodriguez, P. L.; Harada, T.; Christian, D. A.; Pantano, D. A.; Tsai, R. K.; Discher, D. E. Minimal “Self” Peptides that Inhibit Phagocytic Clearance and Enhance Delivery of Nanoparticles. *Science* **2013**, *339*, 971–975.
53. Anselmo, A. C.; Mitragotri, S. Cell-Mediated Delivery of Nanoparticles: Taking Advantage of Circulatory Cells to Target Nanoparticles. *J. Controlled Release* **2014**, *198*, 15–28.
54. Deng, Z. J.; Morton, S. W.; Ben-Akiva, E.; Dreaden, E. C.; Shopsowitz, K. E.; Hammond, P. T. Layer-by-Layer Nanoparticles for Systemic Codelivery of an Anticancer Drug and siRNA for Potential Triple-Negative Breast Cancer Treatment. *ACS Nano* **2013**, *7*, 9571–9584.
55. Poon, Z.; Chang, D.; Zhao, X.; Hammond, P. T. Layer-by-Layer Nanoparticles with a pH-Sheddable Layer for *in Vivo* Targeting of Tumor Hypoxia. *ACS Nano* **2011**, *5*, 4284–4292.
56. Champion, J. A.; Katare, Y. K.; Mitragotri, S. Making Polymeric Micro- and Nanoparticles of Complex Shapes. *Proc. Natl. Acad. Sci. U.S.A.* **2007**, *104*, 11901–11904.